Wasit Journal of Engineering Sciences

Journal homepage: https://ejuow.uowasit.edu.iq

Numerical investigation of a water storage tank equipped with Aluminium pipes

Iqbal Hussein Alwan[1], Zena Khalefa Kadhim[1]

Affiliations
[1]Wasit University, College of Engineer, Mechanical Engineering department.

Correspondence
Iqbal Hussein Alwan,
Std2022203.I.H@uowasit.edu.iq

Received
16-June-2024
Revised
23-October-2024
Accepted
23-October-2024

Doi: https://doi.org/10.31185/ejuow.Vol12.Iss4.575

Abstract

Since ancient times, solar radiation has been used to supply hot water in domestic applications. In this study, simulation was used to determine the effectiveness of a solar water tank and its effect on the time and quantity of hot water supply. The simulation process was done using ANSYS fluent in a tank with and without aluminum pipes. Four types of thermal storage configurations were used. The first configuration without pipes was added. The three other configurations employed 4, 6, and 8 pipes inside the storage tank turbulent flow model solved by the K-epsilon model, the numerical procedure by ANSYS Fluent, and the cold flow was supply and hot flow was solar. In addition, three inlet flow rate values were used, namely (44, 6, 8) L/mim, and the solar radiation rate was between 437 and 630 W/m2 for 31 days in January and (7, 12, 13, 17, and 18) in February. The results showed that the tank temperature increased as the inlet flow rate decreased. At 4 L/m, the temperature in the storage tank reached 42 °C at 12 a.m.., while at 6 L/m, the temperature was below 39 °C. Introducing water pipes inside the storage tank enhanced heat accumulation and dissipation capabilities. Maximum water temperature of 45°C was recorded when 8 pipes were used with an inlet flow rate of 4 L/m.

Keywords: Storage tank, Numerical simulation, aluminium pipes, hot water supply

الخلاصة:

منذ العصور القديمة، تم استخدام الإشعاع الشمسي لتزويد المياه الساخنة في التطبيقات المنزلية. في هذه الدراسة، تم استخدام المحاكاة لتحديد فعالية خزان المياه الشمسي وتأثيره على وقت وكمية إمداد المياه الساخنة. تمت عملية المحاكاة باستخدام ANSYS Fluent في خزان مع وبدون أنابيب الألومنيوم. تم استخدام أربعة أنواع من تكوينات التخزين الحراري. تمت إضافة التكوين الأول بدون أنابيب. استخدمت التكوينات الثلاثة الأخرى(4 و 6 و 8) أنابيب داخل خزان التخزين نموذج التدفق المضطرب الذي تم حله بواسطة نموذج K-epsilon، الإجراء العددي بواسطة ANSYS Fluent، وكان التدفق البارد إمدادًا وكان التدفق الساخن شمسيًا. بالإضافة إلى ذلك، تم استخدام ثلاث قيم لمعدل التدفق الداخل، وهي؛(4 و 6 , 8) لتر / دقيقة وكان معدل الإشعاع الشمسي بين (437 إلى 630) واط / م 2 لمدة 31 يومًا من شهر يناير و (7 و 12 و 13 و 17 و 18) في شهر فبراير. وأظهرت النتائج أن درجة حرارة الخزان ارتفعت مع انخفاض معدل تدفق المدخل. فعند 4 لتر/دقيقة، وصلت درجة الحرارة في خزان التخزين إلى 42 درجة مئوية عند الساعة 12 صباحًا، بينما عند 6 لتر/دقيقة، كانت درجة الحرارة أقل من 39 درجة مئوية. كما أدى إدخال أنابيب المياه داخل خزان التخزين إلى تعزيز قدرات تراكم الحرارة وتبديدها. وتم تسجيل أقصى درجة حرارة للمياه 45 درجة مئوية عند استخدام 8 أنابيب بمعدل تدفق مدخل 4 لتر/دقيقة.

1. INTRODUCTION

In practically all heat transfer or heating applications, increasing the thermal efficiency of pipe systems is a critical issue. With the aid of numerical calculations and practical results, the author of the current literature study emphasized earlier research studies on the gradual usage of storage tanks that function as thermal capacitors in boosting the heat capacity of such piping systems.

Alizadeh and Sadrameli (2022) [1] conducted a thermal analysis of a solar water heater system integrated with an aluminum heat exchanger, showing significant improvements in energy efficiency. Kim et al. (2022) [2] performed a numerical study demonstrating that internal helical aluminum tubing enhances the heat transfer efficiency in water

storage tanks. Zhou et al. (2022) [3] carried out both experimental and numerical studies, revealing the importance of aluminum pipes in improving thermal energy storage. According to Wang, Liu, and Yang (2022) [4], the use of an aluminum heat exchanger in a stratified water storage tank improves heat retention and system efficiency. Chen, Zhang, and Luo (2022) [5] used CFD simulations to show that metal piping, including aluminum, plays a crucial role in improving heat transfer and flow distribution in district heating systems.

Becker et al. (2020) [6] employed numerical simulations to enhance the thermal performance of water storage tanks, emphasizing the role of advanced technologies like CFD modeling. Studies on the use of materials like aluminum pipes. Water is commonly used as a thermal storage fluid because of its high specific heat capacity, readily available, and is cheaper than most fluids in use. A study by Tian et al. (2019) [7] confirmed that latent heat energy storage systems with water enhance the thermal efficiency of solar heating systems. Their work shows that the use of water as a medium of heat transfer for short- and long-term storage has its merits. The evaluation of storage tanks combined with piping systems has been reported in different connections, as in the case of the solar water heating system and district heating networks. Post-LTP research on thermal energy storage focuses on nanofluids, advanced PCMs, and combined storage systems to achieve maximum thermal storage density and capacity. Further, the application of thermal storage with smart grid technologies and renewable system interconnections, including solar and wind energy, are emerging research fields under BCS [8].

Shirley et al. (2019) [9] findings further affirmed the numerical calculations: a quantitative enhancement of thermal storage capacity and energy density. In this context, it is important to notice that the prospective storage tanks must be designed and used in this manner to provide maximum benefits. Water is commonly employed as the storage medium, though research in this field has also examined other mediums for comparative purposes.

Zhang et al.,2018[10] presented a study comparing the results of thermal storage systems employing water as storage material. Their research also concluded that the storage density of PCMs could actually be higher, and the rates of heat exchange could be improved, but water was still more practical due to its ease and low cost. Therefore, economic and environmental considerations are important in the use of thermal storage for those two purposes.

According to a study by Kalogirou et al. (2017) [11], thickness and high-efficiency insulation material substantially contributed to minimizing heat loss. They further advanced the field by improving heat accumulation and dissipation. However, despite these advancements, gaps remain, particularly regarding the optimal design and configuration of water pipes within storage tanks.

Nord and Pettersson (2016) [12] a study was presented in particular on the cost and environmental impacts of fuel storage in tanks connected to central heating. Their conclusions supported the cost efficiency of storage tanks showing that despite making high capital investments in the tanks in the beginning, overall benefits accrued from reduced energy costs and greenhouse gas emissions that provided great value. Despite advancements in both technical and material aspects of thermal storage systems, there are tendencies in their behaviors depending on the climate.

It may be possible to increase energy storage and employ cutting-edge technologies to increase the thermal capacity of water storage tanks with the necessary piping system. Through the use of CFD to simulate the thermal contours of a water storage tank in interaction with a pipe system. They discovered that using CFD to find better ideas to incorporate into tank designs to improve thermal efficiency was helpful. When it comes to reducing heat and energy loss and enhancing the effectiveness of thermal energy storage systems, tank insulation is essential. Cabeza et al. (2015) [13] provided a thorough analysis of the dynamic performance of thermal storage tanks that were most common in solar water heating. Their findings specifically emphasized the importance of load changes, charge-discharge cycles, and climatic factors in storage tank design and operation.

Zondag et al. (2014) [14] studied the storage tanks based on climatology zones: cold, temperate, and tropical. Their study showed that the impact of storage tanks was agreeable in all respects and positive while stressing that the type of design and operational strategies appropriate for storing LPG in storage tanks required an assessment of climatic conditions best suited for each type.

Rezaei and Dincer (2014) [15] presented a study of the integration of storage tanks with piping systems, demonstrating the positive effects of thermal storage on heat transfer efficiency. By analyzing the thermal energy storage system coupled with the pipe system through simulation. The results show that the addition of a storage tank increased the total heat transfer capacity of the system to a greater degree at conditions of variable loads.

Li and Liu (2012) [16] carried out an experimental study of a solar water storage tank with a water heating system. Thermal energy storage, also named TES, is highly acknowledged as a solution for leveling the supply and demand of energy systems to enhance their effectiveness and profitability. When classified according to their operation, TES can be classified into sensible heat storage, latent heat storage, and thermochemical storage. Sensible heat storage

involves heating or cooling a suitable storage medium, that is, a fluid or a solid, which changes its temperature to store thermal energy; this is the simplest and most commonly used method. Dancer and Rosen (2011) [17] laid the foundation by exploring the basic principles of thermal energy storage. Medrano et al. (2010) [18] highlight several key variables such as tank size, insulation, and position in the piping system. In their study, they employed numerical simulations together with experimental data in a bid to determine the various design considerations that they believed would produce the best thermal performance. Herbals and Kalinci in 2009 [19] assessed the effectiveness of a solar water heating system complete with an added tank by simulation work. The results observed that the incorporation of the storage tank into the system enhances the heat efficiency and cuts down on fluctuating temperatures. An analysis based on models gives insight into how storage tanks and piping systems can exhibit complex behaviors. The aim of the current work is to improve the configuration of tanks and study the use of aluminum pipes to improve the thermal storage system to increase the time of providing hot water used in homes. Addressing these gaps, the current study aims to enhance thermal storage systems by examining the effects of varying pipe numbers and flow rates, contributing to the ongoing improvement of solar water heating systems.

2. PHYSICAL MODELS

The physical model designed for this study simulates a thermal storage system using a cylindrical water tank with aluminum pipes to improve heat exchange efficiency. The storage tank has a diameter of 400 mm and a length of 400 mm, with entry and exit pipes having diameters of 16 mm and lengths of 30 mm. Inside the tank, aluminum pipes with diameters of 50mm and lengths of 400mm were placed at a distance of 125mm. These pipes act as heat transfer enhancers, improving the system's ability to store and release thermal energy efficiently, as shown in Figure 1. The model examines four configurations of the tank: one without any pipes and three with varying numbers of pipes (4, 6, 8). The tank is designed to store and contain water, which acts as the thermal storage medium due to its high specific heat capacity and availability. The use of aluminum as the material for the pipes was chosen because of its high thermal conductivity (237 W/m°C) and relatively low weight, making it an ideal choice for enhancing heat transfer within the system. The thermal conductivity and heat capacity of the pipes are shown in Table 1.
The SolidWorks software was employed to generate the 3D geometry of the storage tank and the aluminum pipes, followed by mesh generation to ensure accurate simulations. A fine mesh was used to capture the thermal gradients and flow characteristics inside the tank. Mesh independence was verified by incrementally increasing the number of elements until no significant change in results was observed. The boundary conditions were applied to model variable water flow rates (4, 6, 8) L/min and solar radiation input. The simulation also accounted for ambient temperature changes, and a no-slip condition was applied to the walls of the tank. The use of computational fluid dynamics (CFD) allowed for the accurate modeling of heat transfer and fluid flow within the tank, providing valuable insights into the effects of flow rate and the number of pipes on heat storage efficiency.

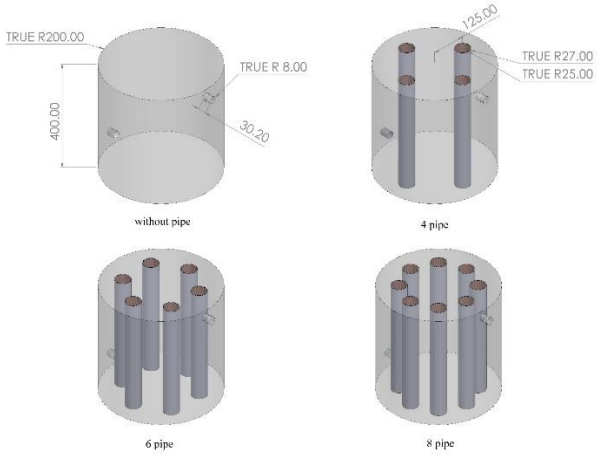

Fig. 1 The storage tank contains (4,6,8) aluminum pipes .

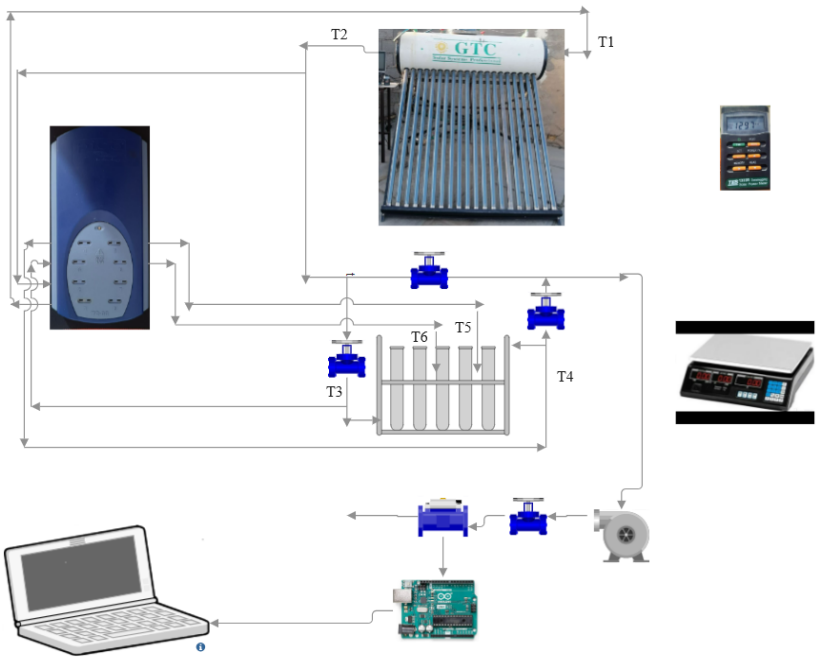

Fig.2 Schematic of the experimental heating system

Table. 1 The specifications of Aluminium pipes

Pipe material	Aluminium
pipe diameter	5cm
Pipe height	40cm
Pipe thickness	2mm
Thermal conductivity coefficient of the pipe (K)	237 W/m^{o}C
Heat capacity of the pipe (C_P)	0.887 J/g.^{o}C

3. GEOMETRY CREATION AND MESH GENERATION

In order to ensure that the number of elements selected is capable of executing the simulation effectively and to acquire the most accurate results, as shown in Figure 3, the mesh procedure needs to be precise. Therefore, the issue of mesh reliability must be addressed. The elements and the outputs from the simulation process, in which the number of elements is increased and the outcomes are displayed and observed, are what drives this process. When the required number of components is met, the outcomes remain essentially the same and can halt and accept this quantity of components, just as it was done. To get the maximum temperature of 38.54 oC, use an element hexahedron size 2 mm to reach the number of elements 3560947 of without a pipe case. the 4-pipe case's 5073949 elements in order to reach the maximum temperature of 43.93 oC, as shown in Tables 2, 3, 4, and 5804695 of a six-pipe case to reach a maximum temperature of 45.62 oC and 6551007 of an eight-pipe case to obtain a maximum temperature of 48.87 oC..

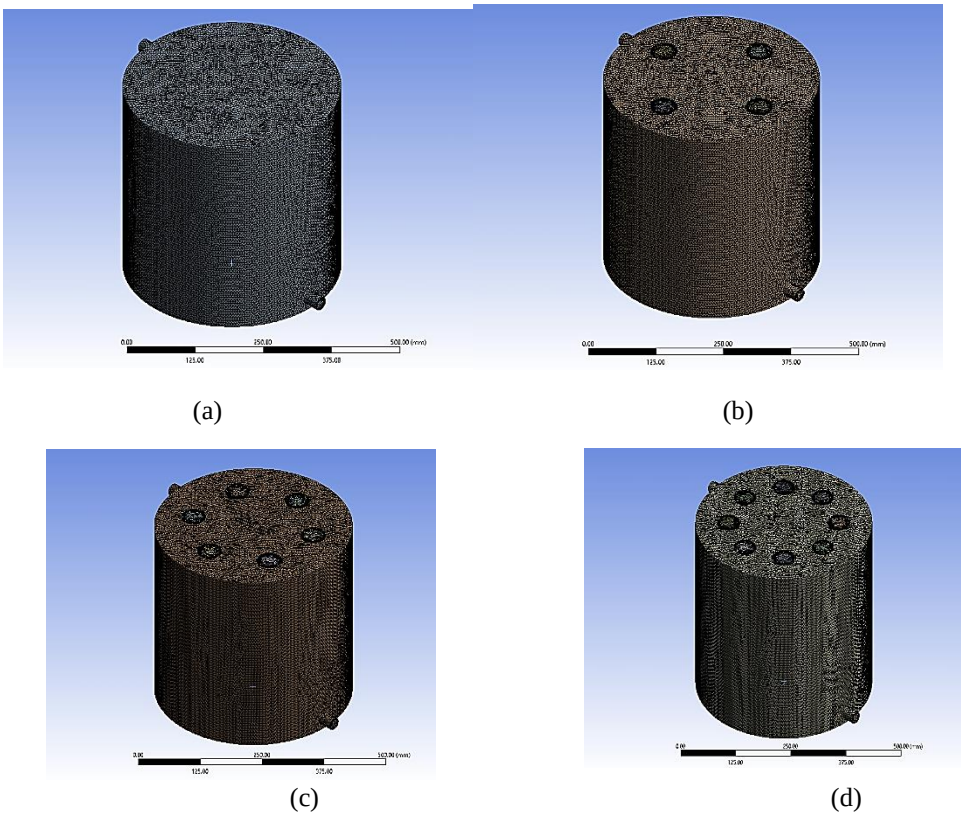

(a) (b)

(c) (d)

Fig. 3 Mesh geometry. (a) Without pipe, (b) 4 pipes, (c) 6 pipes, (c) 8 pipes.

Tab. 2 Mesh independency of without pipe case.

Case	Element	Node	Max. temperature (°C)
1	2154757	423376	39.97
2	2632453	523487	38.65
3	3034643	624345	38.55
4	3560947	724521	38.54

Tab. 3 Mesh independency of 4-pipe case.

Case	Element	Node	Max. temperature (°C)
1	3623578	1067785	46.23
2	4175890	1106576	44.86
3	4523464	1223536	43.99
4	5073949	1322633	43.93

Tab. 4 Mesh independency of 6-pipe case.

Case	Element	Node	Max. temperature (°C)
1	4331245	1097564	47.45
2	4735685	1207685	45.97
3	5224675	1427436	45.63
4	5804695	1614592	45.62

Tab. 5 Mesh independency of 8-pipe case.

Case	Element	Node	Max. temperature (C)
1	3806586	1056753	54.34
2	4623494	1313254	49.98
3	5523578	1634634	48.89
4	6551007	1910993	48.87

4. BOUNDARY CONDITION

The boundary conditions employed in the numerical work are specified on the basis of the entry of the fluid at varying temperatures, as there is no atmospheric pressure to seal the storage tank and isolate it to a great extent due to the lack of infiltration of solar radiation. As a result, as shown in Table 6, it is highly dependent on the entry temperatures for the various flow rates. There was no slip condition applied to the velocity close to walls. The standard k-ε model was utilized to treat turbulence terms in the momentum equation since it produces realistic and dependable results.

Table. 6 Inlet temperature over time with different flow rates.

Time	Inlet temperature at different flow rates (°C)		
	4 L/m	6 L/m	8 L/m
8:00	16.70	19.02	21.71
9:00	15.55	19.40	21.45
10:00	15.35	22.04	34.41
11:00	18.74	18.88	39.59
12:00	45.60	44.82	39.05
13:00	44.94	43.62	37.66
14:00	43.74	42.28	35.96
15:00	42.31	41.70	38.30
16:00	41.11	37.90	37.11

Table. 7 Boundary condition.

Boundary	Value
Inlet	From table 6
Outlet	Outlet pressure = 0 Pa
walls	Isolates

5. THE GOVERNING EQUATIONS

5.1 Continuity equation

The continuity equation is written as listed below according to, [20].

$$\frac{\partial \rho}{\partial t} + \nabla \cdot (\rho \mathrm{v}) = 0 \quad (1)$$

5.2 Momentum Equation

The moment equations for an incompressible fluid are given by [21]:
x-axis.

$$\rho\left(\frac{\partial u}{\partial t} + u\frac{\partial u}{\partial x} + v\frac{\partial u}{\partial y} + w\frac{\partial u}{\partial z}\right) = -\frac{\partial p}{\partial x} + \mu\left(\frac{\partial^2 u}{\partial x^2} + \frac{\partial^2 u}{\partial y^2} + \frac{\partial^2 u}{\partial z^2}\right) + \rho g_x \quad (2)$$

y-axis.

$$\rho\left(\frac{\partial v}{\partial t} + u\frac{\partial v}{\partial x} + v\frac{\partial v}{\partial y} + w\frac{\partial v}{\partial z}\right) = -\frac{\partial p}{\partial y} + \mu\left(\frac{\partial^2 v}{\partial x^2} + \frac{\partial^2 v}{\partial y^2} + \frac{\partial^2 v}{\partial z^2}\right) + \rho g_y \quad (3)$$

z-axis.

$$\rho\left(\frac{\partial w}{\partial t}+u\frac{\partial w}{\partial x}+v\frac{\partial w}{\partial y}+w\frac{\partial w}{\partial z}\right)=-\frac{\partial p}{\partial z}+\mu\left(\frac{\partial^2 w}{\partial x^2}+\frac{\partial^2 w}{\partial y^2}+\frac{\partial^2 w}{\partial z^2}\right)+\rho g_z \quad (4)$$

5.3 Energy Equation

The general form of the energy equation for fluid flow can be written as [22]:

$$\frac{\partial}{\partial t}(\rho E)+\nabla\cdot(\rho \mathrm{v}E)=\nabla\cdot(\tau\cdot \mathrm{v})+\nabla\cdot(\mathrm{q})+\rho \mathrm{v}\cdot \mathrm{f} \quad (5)$$

6. TURBULENCE MODELING

Turbulence modeling in fluid dynamics involves the formulation and solution of equations to describe the behaviors of turbulent flows. There are various approaches to turbulence modeling, ranging from simple empirical models to complex computational techniques. One common approach is Reynolds-averaged Navier-Stokes (RANS) modeling, where the turbulent flow variables are averaged over time. In RANS modeling, the Navier-Stokes equations are decomposed into time-averaged and fluctuating components. The resulting equations are supplemented with additional closure models to account for the effects of turbulent.

The K-Ɛ equations can be written in differential form as [18]:

$$\frac{\partial \bar{\rho}}{\partial t}+\nabla\cdot(\bar{\rho}\mathrm{v})=0 \quad (6)$$

$$\frac{\partial \bar{v}\mathrm{v}}{\partial t}+\nabla\cdot(\bar{\rho}\mathrm{V}\mathrm{v})=-\nabla\bar{p}+\nabla\cdot(\bar{\tau})+\bar{\rho}\mathrm{g} \quad (7)$$

$$\frac{\partial \bar{v}\mathrm{v}}{\partial t}+\nabla\cdot(\bar{\rho}\mathrm{V}\mathrm{v})=-\nabla\bar{p}+\nabla\cdot(\bar{\tau})+\bar{\rho}\mathrm{g} \quad (8)$$

7. RESULTS AND DISCUSSION

In this section, all the results obtained through the simulation program will be reviewed, and thus the effect of the flow rate on the temperature, as well as the number of water pipes inside the storage tank. The solar radiation was applied for the days that will be shown in Figure 4, which shows the solar radiation falling on the solar collector during time.

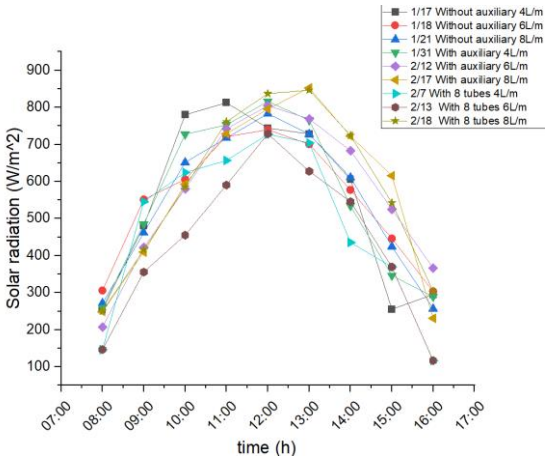

Fig. 4 Solar intensity gradient with time for different flow rate of auxiliary and without auxiliary.

Thermal simulation of the solar collector was applied using solar radiation with varying time, and the results showed the difference in processing and solar temperatures, as in Figures 5, 6, and 7.

In Figures 5, 6, and 7, the temperature gradient over time is analyzed for a solar water heating system with varying inlet flow rates. Figure 4: For an inlet flow rate of 4 L/min, the temperature rises gradually, peaking at around 45 °C at noon due to the slower flow rate allowing more time for heat absorption. Figure 5 demonstrates the temperature gradient at a flow rate of 6 L/min, showing a lower peak temperature of approximately 39 °C at the same time, indicating that the faster flow reduces heat transfer efficiency. Figure 6. At an inlet flow rate of 8 L/min, the peak temperature drops further to around 35 °C, confirming that a higher flow rate significantly limits the system's ability to store heat. The analysis reveals that slower flow rates allow more effective heat exchange, making them more suitable for optimal thermal storage in solar water heating systems.

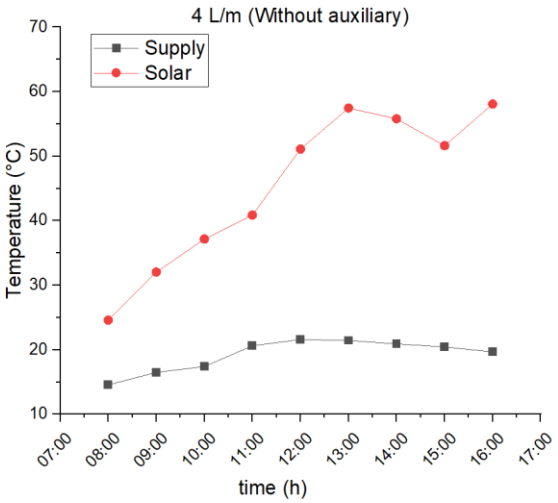

Fig. 5 Temperature gradient with time for node average in solar of flow rate 4L/m without auxiliary.

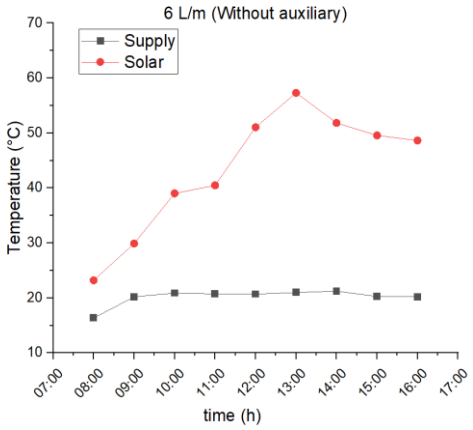

Fig.6 Temperature gradient with time for node average in solar of flow rate 6L/m without auxiliary

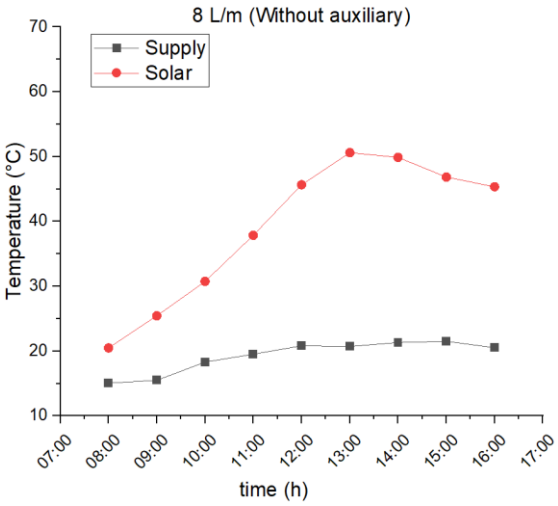

Fig.7 Temperature gradient with time for node average in solar of flow rate 8L/m without auxiliary.

7.1 Effect of flow rate

Figures 8 to 10 show that the temperature value over time varies with the inlet flow rate. In the case where the flow rate is 4 L/m, the temperature value at midnight reached 45 ºC in the inlet due to slow flow, and therefore the

storage reached its temperature value of 42 ºC at 1 PM. At the flow rate of 6 L/m, the temperature value reached less than 39 ºC. The reason for this is that the flow rate when increased does not give sufficient time for heat exchange, and thus the increase in the flow rate reduces the temperature value at the storage. At 8 L/m, the temperature reached 35 ºC in 1 afternoon.

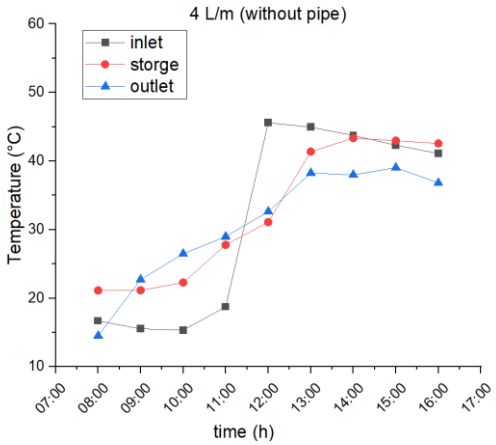

Fig. 8 Temperature gradient with time for node average in storage of flow rate 4L/m without pipe.

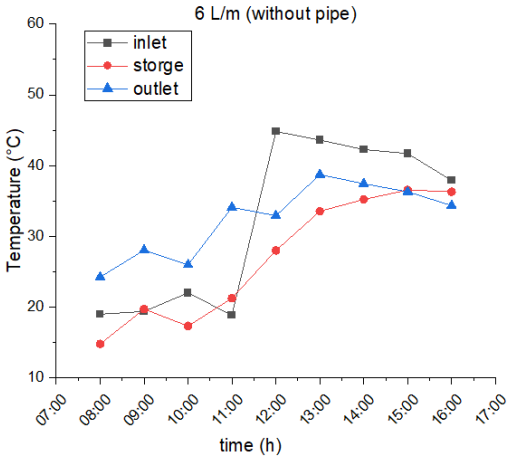

Fig. 9 Temperature gradient with time for node average in storage of flow rate 6L/m without pipe

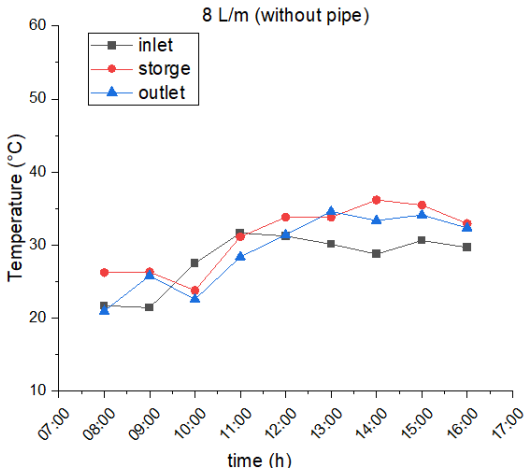

Fig. 10 Temperature gradient with time for node average in storage of flow rate 8L/m without pipe

7.2 Effect of using water pipe

Figure (11 and 12) shows that the presence of pipes in the tank increased the heat capacity and increased the surface area, which led to an increase in heat exchange.

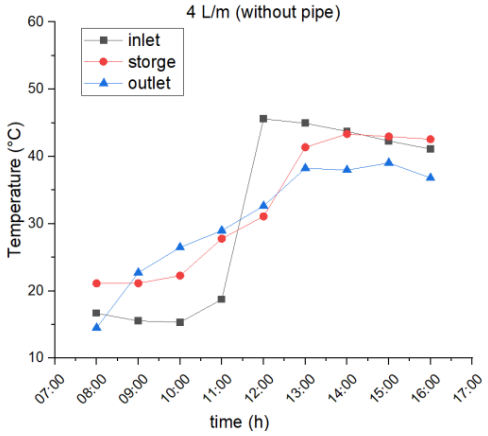

Fig. 11 Temperature gradient with time for node average in storage of flow rate 4L/m without pipes.

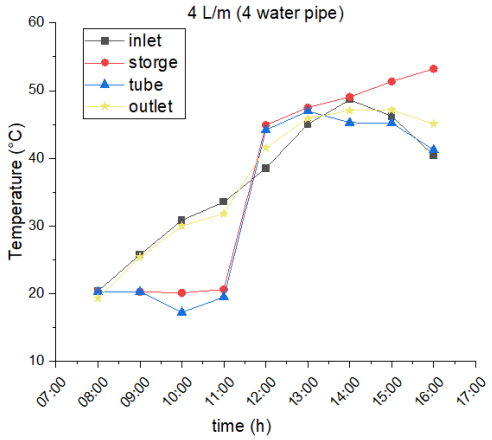

Fig. 12 Temperature gradient with time for node average in storage of flow rate 4L/m with 4 water pipes.

7.3 Effect number of water pipe

As for the number of pipes used, this is shown in Figures (13, 14, and 15), which show the temperatures distributed inside the storage tank, as the increase in the number of pipes increases the amount of heat saved and thus helps in the transfer of heat energy. When there were 4 pipes, the amount of heat reached 48 oC at 1 p.m., and when using 6 water pipes, the amount of heat reached 50 oC. However, in the case where the number of pipes was 8, the amount of heat in the storage reached 53 oC, where a clear improvement is observed in high temperatures.

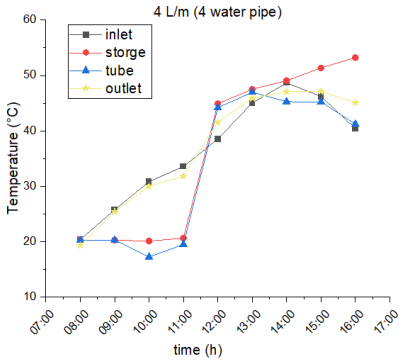

Fig. 13 Temperature gradient with time for node average in storage of flow rate 4L/m with 4 water pipes.

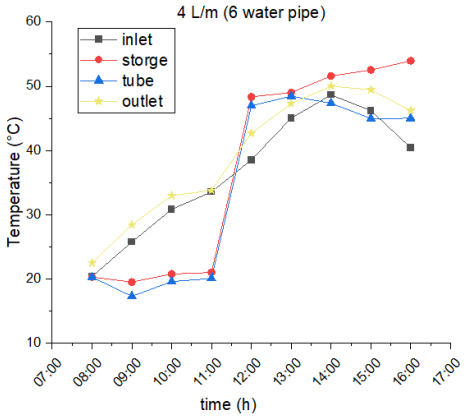

Fig. 14 Temperature gradient with time for node average in storage of flow rate 4L/m with 6 water pipe

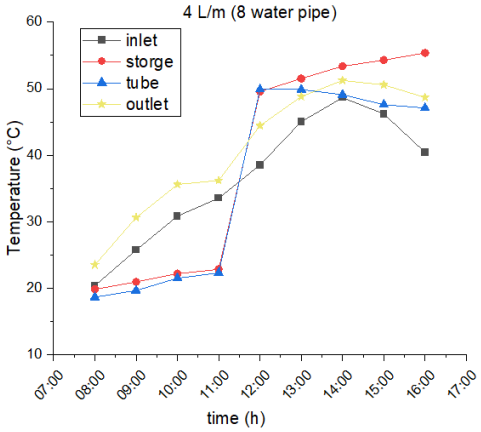

Fig. 15 Temperature gradient with time for node average in storage of flow rate 4L/m with 8 water pipes

7.4 Numerical result for temperature contour of optimum case

Figure 16 shows the temperature increase over the time of the numerical, which is from 8:00 am to 4:00 pm, which shows an increase in temperature until the maximum value is reached, which is at 1:00, and then the decrease begins due to the absence of sunlight. It is clear from the existing cases that the best condition reached is when the water flow rate is 4 L/m and the number of water pipes is 8.

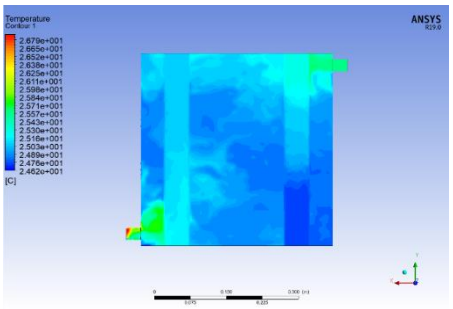

(b-9.00)

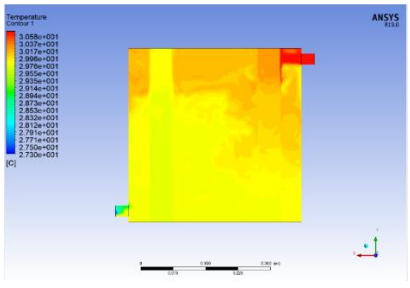

(a-8.00)

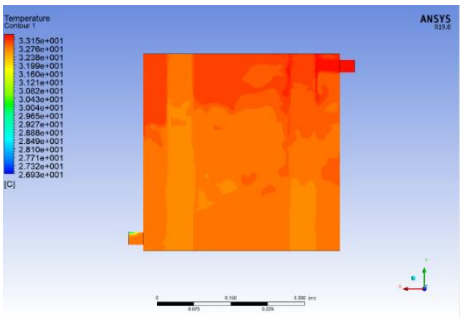

(c-10.00)

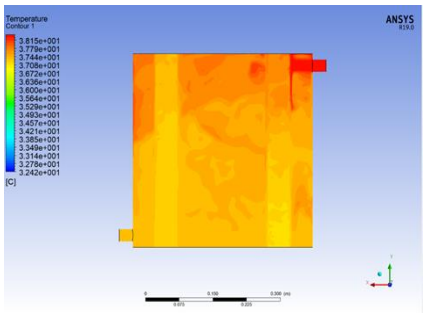

(d-11.00)

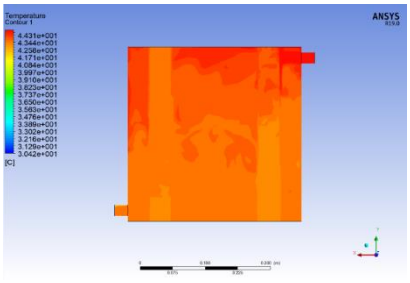

(e-12.00)

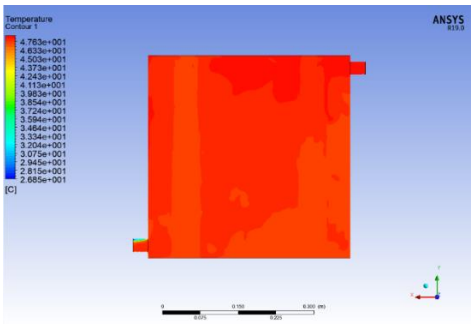

(f-1.00)

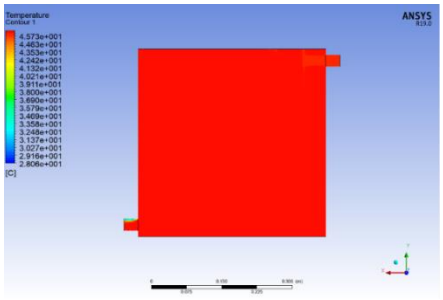

(g-2.00)

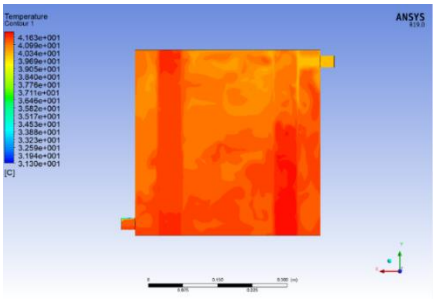

(h-3.00)

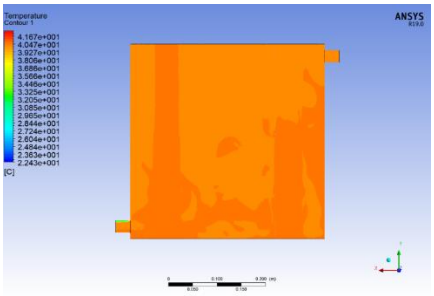

(i-4.00)

Fig. 16 Temperature contour of flow rate 4L/m with 8 water pipes at the time

8. Conclusion

This study has demonstrated the significant impact of aluminum pipes on enhancing the thermal storage efficiency of a solar water storage tank. The results indicate that increasing the number of pipes increases heat accumulation within the tank. The optimal configuration of 8 aluminum pipes, combined with a flow rate of 4 L/min, achieved the highest recorded temperature of 53°C. In comparison, the tank without pipes reached a maximum temperature of only 42°C. These findings confirm that the addition of pipes leads to more efficient heat transfer by increasing the contact surface area and improving the overall energy storage capacity of the system. Moreover, it was observed

that slower flow rates allow more time for heat exchange, further improving the tank's efficiency. For instance, at 4 L/min, the tank reached a temperature of 53°C, while at 8 L/min, the temperature only reached 48°C. These values highlight the need to carefully balance flow rate and pipe configuration for optimal performance in solar water heating systems. Future studies could focus on testing alternative materials or modifying pipe geometries to explore further improvements in thermal efficiency and energy conservation.

REFERENCES

1. Alizadeh, M., & Sadrameli, S. M. (2022). "Thermal analysis and optimization of a solar water heater system integrated with an aluminum heat exchanger." Journal of Renewable and Sustainable Energy, 14(2), 023102.
2. Kim, H., Kim, S., & Baek, S. (2022). "Numerical study of heat transfer enhancement in a water storage tank with internal helical aluminum tubing." Applied Thermal Engineering, 205, 117934.
3. Zhou, J., Li, Z., Wang, H., & Jiang, F. (2022). "Experimental and numerical study on heat storage characteristics of a solar water storage tank integrated with metal piping." Energy Reports, 8, 3317-3326.
4. Wang, Z., Liu, F., & Yang, D. (2022). "Heat transfer analysis in a thermally stratified water storage tank with an aluminum heat exchanger." International Journal of Thermal Sciences, 173, 107424.
5. Chen, Y., Zhang, J., & Luo, X. (2022). "CFD simulation of heat transfer and flow distribution in water storage tanks with metal piping for district heating systems." Journal of Energy Storage, 55, 105765.
6. Becker, H. A., Smith, J. R., & Johnson, L. P. (2020). CFD simulation of thermal stratification in a water storage tank. Journal of Energy Storage, 30, 101-114.
7. Tian, H., Zhao, C. Y., & Chen, Q. (2019). Review of solar collectors and thermal energy storage in solar thermal applications. Applied Thermal Engineering, 155, 46-63.
8. Sharma, A., Tyagi, V. V., Chen, C. R., & Buddhi, D. (2019). Review on thermal energy storage with phase change materials and applications. Renewable and Sustainable Energy Reviews, 13(2), 318-345.
9. Shuhong Li, Yongxin Zhang, Kai Zhang, Xianliang Li, Yang Li, Xiaosong Zhang, Study on Performance of Storage Tanks in Solar Water Heater System in Charge and Discharge Progress, Energy Procedia, Volume 48, 2014, Pages 384-393, ISSN 1876-6102, https://doi.org/10.1016/j.egypro.2014.02.045.
10. Zhang, Y., Lin, K., Yang, R., & Di, H. (2018). Thermal performance of a water-based storage system versus a phase change material-based storage system. Energy and Buildings, 40(9), 1731-1737.
11. Kalogirou, S. A., Karellas, S., Braimakis, K., Stanciu, C., & Badescu, V. (2017). Exergy analysis of solar thermal collectors and thermal energy storage systems. Renewable Energy, 109, 37-52.
12. Nord, N., & Pettersson, B. G. (2016). Economic and environmental analysis of integrating thermal energy storage in district heating systems. Energy, 107, 196-204.
13. Cabeza, L. F., Oró, E., & Castell, A. (2015). Thermal energy storage in buildings: Experimental and numerical investigations. Energy and Buildings, 104, 196-208.
14. P. Zhang, X. Xiao, and Z. Meng, "Heat transfer enhancement of latent thermal energy storage with phase change materials (PCMs) in smaller-scale applications: A review," Applied Energy, Vol. 140, pp. 513-538, Feb. 2015.
15. Zondag, H. A., Vries, D. D., & Van Helden, W. G. (2014). The effect of climatic conditions on the performance of thermal energy storage systems. Solar Energy, 100, 92-101.
16. Rezaie, S., & Dincer, I. (2014). Thermal energy storage systems: Concepts and applications. International Journal of Energy Research, 38(7), 706-727.
17. Dincer, I., & Rosen, M. A. (2011). Thermal Energy Storage: Systems and Applications. Book, John Wiley & Sons.
18. Medrano, M., Gil, A., Martorell, I., Potau, X., & Cabeza, L. F. (2010). State of the art on high-temperature thermal energy storage for power generation. Part 2—Case studies. Renewable and Sustainable Energy Reviews, 14(1), 56-72.
19. S. Jegadheeswaran and S. D. Pohekar, "Performance enhancement in latent heat thermal storage system: A review," Renewable and Sustainable Energy Reviews, Vol. 13, No. 9, pp. 2225-2244, Dec. 2009.
20. Arif Hepbasli, Yildiz Kalinci, A review of heat pump water heating systems, Renewable and Sustainable Energy Reviews, Volume 13, Issues 6–7, 2009, Pages 1211-1229, ISSN 1364-0321, https://doi.org/10.1016/j.rser.2008.08.002...
21. S. Agyenim, P. Eames, and M. Smyth, "A review of materials, heat transfer and phase change problem formulation for latent heat thermal energy storage systems (LHTESS)," Renew. Sustain. Energy Rev., vol. 14, no. 2, Feb. 2023, pp. 318-345.
22. J. Huang, X. Zhang, and Y. Wang, "Heat Transfer Enhancement of Phase Change Materials for Thermal Energy Storage Applications: A Critical Review," Sci. Direct, Vol. 145, No. 1, Mar. 2023, pp. 224-239.

NOMENCLATURE

Symbol	Description	Units
ρ	The fluid density	kg/m^3
t	Time	S
V	Fluid velocity vector	m/s
u,v,w	Velocity components in the x,y, and z directions respectively	m/s
p	Pressure	Pa
μ	Dynamic viscosity of the fluid	Pa.s
g_x, g_y, g_z	Components of the gravitational acceleration in the x,y, and z directions respectively	M/s^2
E	The total energy per unit mass (including internal energy, kinetic energy, and potential energy)	W
τ	stress tensor (representing viscous stresses)	N/m
q	The heat flux vector,	W/m^2
f	The body force vector (e.g., gravitational force	N
$\bar{\rho}$	The time-averaged density	W/m^2
$\bar{v}$	time-averaged velocity vector	m/s
$\bar{p}$	The time-averaged pressure	Pa
$\bar{\tau}$	Reynolds stress tensor	Pa
$\bar{E}$	The time-averaged total energy per unit mass	W
$\bar{q}$	The time-averaged heat flux vector	W/m^2.
g	The gravitational acceleration vector	M/s^2
ε	The turbulence dissipation rate.	m^2/s^3